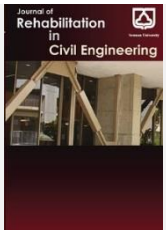

Journal of Rehabilitation in Civil Engineering

Journal homepage: https://civiljournal.semnan.ac.ir/

Prediction of Coefficient of Restitution of Limestone in Rockfall Dynamics Using Adaptive Neuro-Fuzzy Inference System and Multivariate Adaptive Regression Splines

Amir Hossein Shafiee [1,*]; Nima Aein [2]

1. Assistant Professor, Faculty of Civil Engineering and Architecture, Shahid Chamran University of Ahvaz, Ahvaz, Iran
2. Assistant Professor, Department of Civil Engineering, Dariun Branch, Islamic Azad University, Dariun, Iran
* Corresponding author: *am.shafiee@scu.ac.ir*

ARTICLE INFO

Article history:
Received: 19 October 2024
Revised: 30 May 2025
Accepted: 01 July 2025

Keywords:
Coefficient of restitution;
Adaptive neuro-fuzzy inference system;
Rockfall;
Field test;
Multivariate Adaptive Regression Splines (MARS).

ABSTRACT

Rockfalls are a type of landslide that poses significant risks to roads and infrastructure in mountainous regions worldwide. The main objective of this study is to predict the coefficient of restitution (COR) for limestone in rockfall dynamics using an adaptive neuro-fuzzy inference system (ANFIS) and Multivariate Adaptive Regression Splines (MARS). A total of 931 field tests were conducted to measure kinematic, tangential, and normal CORs on three surfaces: asphalt, concrete, and rock. The ANFIS model was trained using five input variables: impact angle, incident velocity, block mass, Schmidt hammer rebound value, and angular velocity. The model demonstrated strong predictive capability, achieving root mean square errors (RMSEs) of 0.134, 0.193, and 0.217 for kinematic, tangential, and normal CORs, respectively. These results highlight the potential of ANFIS to handle the complexities and uncertainties inherent in rockfall dynamics. The analysis was also extended by fitting a MARS model (degree 2, 8 basis functions) to the same dataset. The MARS model achieved MAE ≈ 0.095 and RMSE ≈ 0.118—marginally improving over ANFIS—while delivering a fully explicit algebraic form and an intrinsic ranking of variable importance.

E-ISSN: 2345-4423

How to cite this article:
Shafiee, A. H. and Aein, N. (2026). Prediction of Coefficient of Restitution of Limestone in Rockfall Dynamics Using Adaptive Neuro-Fuzzy Inference System and Multivariate Adaptive Regression Splines. Journal of Rehabilitation in Civil Engineering, 14(2), 2168 http://doi.org/10.22075/jrce.2025.2168

1. Introduction

Roads and structures in mountainous regions are typically prone to rockfalls. [1–6]. Intense rainfall, natural or human-induced undercutting of the slope, and earthquake shaking are the main reasons for such potentially damaging hazards. Some studies were carried out to assess the stability of rock slopes using slope mass rating [7,8]. Rock blocks may bounce, roll, or slide after each impact with the ground surface. Mitigation techniques such as creating berms on the slope, excavating ditches, and constructing barriers on the toe are most efficient when the trajectory of falling rocks can be predicted as accurately as possible. The critical parameter for determining the motion path of falling rocks is the coefficient of restitution (COR). This coefficient is embedded as an input parameter in rockfall analysis software such as RocFall [9] and CRSP [10]. The kinematic COR (R_v) is defined as the ratio of the rebound velocity (v_r) to incident velocity (v_i) (Fig. 1):

$$R_v = \frac{v_r}{v_i} \tag{1}$$

Energy loss always occurs during impact. This loss could happen in the form of the generation of heat, stress waves, and sound energy [11]. As a result, the R_v coefficient can have values between zero and one. Zero R_v corresponds to a perfectly plastic impact, whereas unit R_v corresponds to a perfectly elastic impact. It is also common to define COR as the ratio of tangential and normal components of the velocities. The tangential COR (R_t) is determined by:

$$R_t = \frac{v_{t,r}}{v_{t,i}} \tag{2}$$

where $v_{t,i}$ and $v_{t,r}$ are tangential components of the incident and rebound velocities, respectively (Fig. 1).

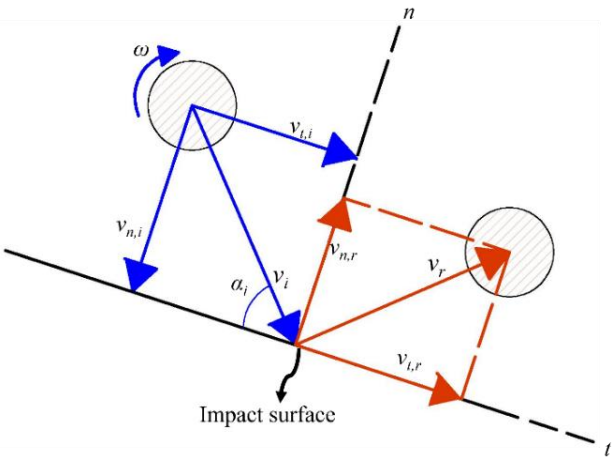

Fig. 1. Parameters used in COR definition.

Similarly, the normal COR (R_n) is defined as the ratio of the normal component of rebound velocity ($v_{n,r}$), to the normal component of the incident velocity ($v_{n,i}$) as follows:

$$R_n = \frac{v_{n,r}}{v_{n,i}} \tag{3}$$

Several experimental studies were conducted to calculate the coefficients, as mentioned earlier, and to determine the influencing factors. Most of these tests were performed in the laboratory [12–19], and some of them were conducted in the field [20–22]. In the laboratory tests, a mechanical throwing apparatus was built to throw small diameter pieces of rock or other materials under completely controlled conditions.

Although these controlled conditions allow scholars to study the effect of various parameters more accurately, it could be much different from the actual rockfall event in nature. For example, the thrown objects in laboratory tests often had unique shapes, such as spherical [15,16] or cubic [20]. In contrast, the natural shape of falling rocks in real rockfall scenarios can be very irregular. Some laboratory tests were also performed on materials other than rock, such as concrete [12], cement [16] or gypsum [14]. The field tests have their difficulties and limitations, too. The conditions are less controlled than laboratory tests, and a vast amount of uncertainty may be included in the tests. However, the process of rockfall in field tests is more similar to the actual conditions.

Many efforts have been made to determine the influencing factors on the R_t, R_n, and R_v coefficients. Ji et al. [17] classified these factors as impact angle (α_i in Fig. 1), incident velocity (v_i in Fig. 1), block size or mass, Schmidt hammer rebound value of impact surface (R_{surf}) and block, and rotational speed (ω). However, the results of previous tests published in the literature showed multiple contradictions, such as:

a) While the majority observed that α_i had a decreasing effect on R_n [16,17,20], Tang et al. [19] observed several cases where R_n increased with an increase in α_i value. The effect of impact angle on R_t was even more inconsistent. Asteriou [16] reported that the R_t coefficient increased by an increase in this angle, whereas Ji et al. [17] observed that α_i had decreasing effect on R_t. Moreover, Asteriou et al. [20] showed that the α_i versus R_t data were highly scattered and did not follow any specific trend.

b) Scholars such as Asteriou [16] and Ji et al. [23] found out that both R_t and R_n coefficients were not sensitive to variation of ω, whereas Buzzi et al. [12] observed the increasing effect of ω on these coefficients. Besides, Ji et al. [17] mentioned that although ω had an increasing effect on the R_t and R_v coefficients, it did not have a significant influence on R_n.

c) The effect of block mass on COR was controversial, too. Some studies [15,16] reported that the R_n coefficient decreased with an increase in block mass, and some others [22] pointed out that there was no clear trend between the variations of R_n and block mass.

The contradictions above, show very well the enormous uncertainty and vagueness that exist in the standard technique of measurement of COR, and the complex nature of impact by itself. The possible reasons for these uncertainties are discussed at section 4 of this paper.

Despite the critical importance of accurately predicting the COR for modeling rockfall dynamics, the literature predominantly relies on empirical relationships or laboratory-scale tests. Limited studies have employed field tests to determine COR, and there is a notable lack of research applying machine learning techniques, such as the Adaptive Neuro-Fuzzy Inference System (ANFIS), for this purpose. This study addresses these gaps by utilizing ANFIS to develop a predictive model for COR of limestone based on field test data. The ANFIS was chosen for this study due to its ability to combine the interpretability of fuzzy logic with the learning capability of neural networks. This hybrid approach makes ANFIS particularly suitable for modeling complex, nonlinear relationships, such as those governing the coefficient of restitution in rockfall dynamics. Unlike traditional regression techniques, ANFIS provides explicit rules that can be interpreted and refined based on domain knowledge, offering both accuracy and transparency. To the best of the authors' knowledge, this is the first application of ANFIS or any machine learning technique for predicting COR in rockfall contexts. Additionally, the reliance on field tests ensures that the derived model is directly applicable to real-world scenarios.

In the following of this paper, the ANFIS is discussed at first. Next, the experiments program of this study and the obtained results are presented in detail. Then, the application of ANFIS for the prediction of COR is fully explained. At last, the concluding remarks are mentioned in the final section of this paper.

2. Fuzzy sets and ANFIS

The fuzzy logic, first presented by Zadeh [24], is a powerful tool for representing uncertainties that are not random, but are associated with a lack of information, vagueness, or imprecision [25]. The fuzzy inference system can estimate the outputs from several inputs, even in complex systems. This system includes the following steps:

1. Some membership functions are assigned to each parameter (either input or output). The membership functions may have different shapes, such as triangular, trapezoidal, or Gaussian. These functions must have values between zero and one in their entire domain. The number, shape, and value of membership functions should be selected based on data values and, of course, a wise judgment. This process is called fuzzification.
2. Then, some rules must be defined between the membership functions of input variables (x_1, x_2, ..., x_k, ..., ...x_n) and output (y) data. The general form of these rules is as follows:

Rule k: If x_1 is A_{1k}, and, or x_2 is A_{2k}, …, and, or x_n is A_{nk}, then y is B_k (4)

where A_{1k}, A_{2k}, A_{nk}, and B_k denotes the fuzzy sets corresponding to x_1, x_2, x_n, and y.

3. Now, the membership function corresponding to each rule ($\mu(x, y)$) must be obtained using an implication operator. One of the most common implication techniques is called the Mamdani implication [26], and is represented as follows:

$$\mu(x, y) = \min[\mu_A(x), \mu_B(y)] \quad (5)$$

where $\mu_A(x)$ and $\mu_B(y)$ are membership functions relating to the antecedent and consequent of the rule.

4. In the next step, the membership functions of each rule (derived from step 3) are aggregated to form a unique membership function. The aggregation procedure can be performed using either the maximum or summation approach.
5. In this step, defuzzification is performed, where the resulting fuzzy set is converted into a crisp number. Several methods can be used for defuzzification, including the centroid method, the bisector method, the mean of maximums, and others.

If the output (y) in Eq. (4) is defined as a function, not a fuzzy set, the resulting system is called the Sugeno system [27]. The ANFIS, first proposed by Jang [28], is a Sugeno-type fuzzy inference system in which the y is defined as a linear function of fuzzy inputs. For example, for a simple system with two inputs x_1 and x_2, and two rules:

Rule 1: If x_1 is A_{11} and x_2 is A_{21}, then $y_1 = p_1 x_1 + q_1 x_2 + r_1$ (6)

Rule 2: If x_1 is A_{12} and x_2 is A_{22}, then $y_2 = p_2 x_1 + q_2 x_2 + r_2$ (7)

The ANFIS is described in five layers, as shown in Fig. 2. In the first layer, x_1 and x_2 are defined as fuzzy sets. So, the membership

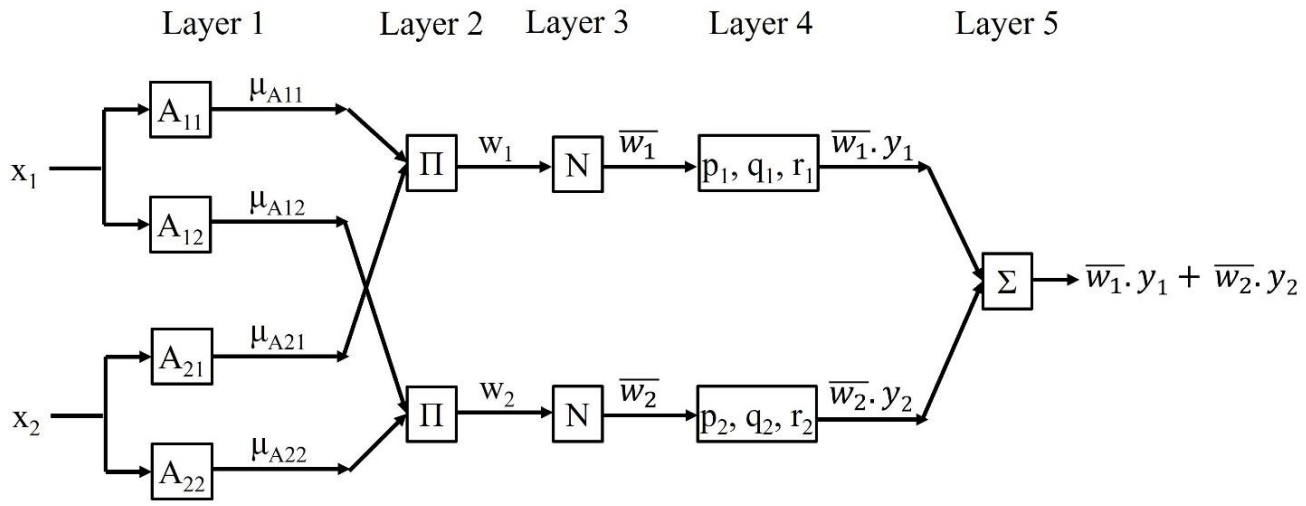

Fig. 2. ANFIS architecture.

functions $\mu_{A11}(x_1)$, $\mu_{A12}(x_1)$, $\mu_{A21}(x_2)$, $\mu_{A22}(x_2)$ are the result of this layer.

In the second layer, the weight factors (w_1 and w_2) are obtained using the following equations:

$$w_i = \mu_{A1i}(x_1) \times \mu_{A2i}(x_2) \qquad i = 1, 2 \tag{8}$$

The weight factors are normalized in the third layer as follows:

$$\overline{w_i} = \frac{w_i}{\sum_{j=1}^{2} w_j} \tag{9}$$

In the fourth layer, each normalized weight factor is multiplied by the corresponding output function, resulting in $\overline{w_i}.y_i$. Finally, the predicted output of ANFIS is determined in the fifth layer by:

$$y = \sum_{i=1}^{2} \overline{w_i}.y_i \tag{10}$$

In ANFIS, a learning process adjusts the parameters related to the shape of membership functions of the training data automatically. This adjustment aims to minimize the error between the observed and predicted outputs. In recent years, the ANFIS has been implemented in several engineering and geotechnical problems [29–33]. The architecture of ANFIS, as illustrated in Fig. 2, is particularly suitable for COR determination due to its ability to integrate diverse inputs, such as impact angle and surface properties, while accounting for the inherent uncertainties in rockfall dynamics. This adaptability ensures robust predictions even in complex field scenarios.

3. Multivariate adaptive regression splines

Multivariate Adaptive Regression Splines (MARS) is a flexible, nonparametric regression technique introduced by Friedman [34]. It models complex nonlinear relationships by fitting piecewise-linear segments (splines) joined at automatically determined knots, and by selecting only those segments that improve predictive performance. MARS builds its model from one or more hinge basis functions, each of which "activates" on one side of a knot point x_0. A single hinge is defined as:

$$b(x; x_0) = \max(0, x - x_0) \text{ or } \max(0, x_0 - x) \tag{11}$$

Fig. 3 illustrates how a single MARS hinge at x_0 transforms a noisy dataset into a piecewise-linear fit.

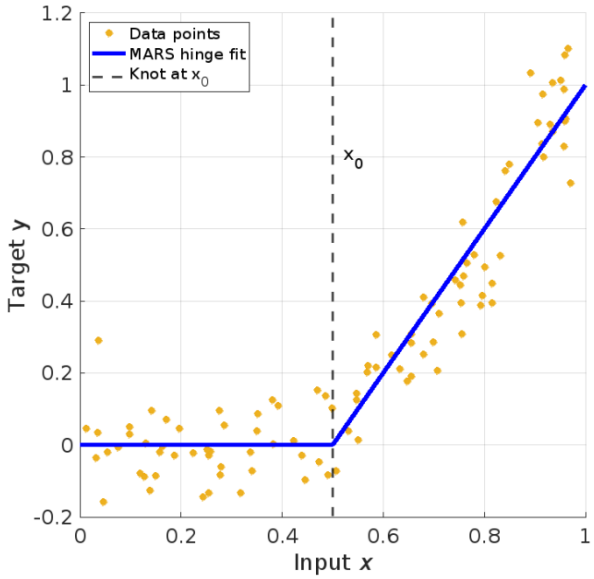

Fig. 3. Illustration of hinge basis functions.

By taking products of these hinge functions across different inputs, MARS can capture interactions of arbitrary order. Starting from a constant intercept c_0, MARS adds pairs of hinge functions in a forward phase, choosing at each step the candidate that most reduces training error. Once the model is over-grown, a backward pruning phase deletes the least useful basis functions one at a time. The final model has the form:

$$f(x) = c_0 + \sum_{i=1}^{N} c_i . BF_i(x) \tag{12}$$

where each $BF_i(x)$ is either a single hinge $b(x_j; x_0)$ or a product of up to H hinges (interaction degree), and c_i are the learned coefficients. We control the maximum interaction degree as a hyperparameter.

To avoid overfitting, MARS uses Generalized Cross-Validation (GCV) during pruning. For a dataset of m observations and a model with n basis functions (excluding the intercept), and smoothing factor d (default: 3), the GCV score is defined as:

$$GCV = \frac{\frac{1}{m}\sum_{i=1}^{m}[y_i - f(x)]^2}{\left(1 - \frac{n + \frac{d(n-1)}{2}}{m}\right)^2} \tag{13}$$

Minimizing GCV balances goodness-of-fit (mean squared error) against model complexity (number of knots and basis functions). In our implementation, we choose the number of basis functions N at the "elbow" of the GCV vs. N curve, where additional terms yield negligible GCV improvement.

An additional benefit of MARS is an intrinsic variable importance measure. For each predictor j, we remove all basis functions involving x_j and recompute GCV, yielding:

$$\Delta GCV_j = GCV_{without\ j} - GCV_{full} \tag{14}$$

The relative importance (RI) is then normalized so the largest ΔGCV receives 100% [35]:

$$RI_j = \frac{\Delta GCV_j}{max_{k=1,\ldots,p}\Delta GCV_k} \tag{15}$$

This ranking provides clear insight into which variables drive model performance.

MARS combines interpretability and flexibility in a way few other nonlinear techniques can match. By expressing its model as an explicit sum of piecewise-linear basis functions, it yields a clear, algebraic equation that can be inspected and even embedded directly into engineering calculations. The knot locations and hinge directions are chosen automatically—there's no need to hand-tune partitions or membership functions—while a backward-pruning step guided by generalized cross-validation (GCV) removes any basis functions that don't improve predictive accuracy. This same GCV criterion also provides a built-in ranking of variable importance, allowing one to see which inputs matter most. Finally, by specifying the maximum degree of interaction, MARS can capture both additive and higher-order effects. In recent years, MARS has been employed in various geotechnical problems [36–42].

4. Experimental program

The experiments were conducted at the toe of a rocky slope in Shiraz, Iran. In recent years, multiple landslides and rockfalls occurred in this region, such as the one in December 2018, in which a colossal rock block fell on the roof of a residential building and made a big hole in it [5]. The experimental area was located at a latitude of 29° 39′ 32″, and a longitude of 52° 29′ 33″. This point was selected because it included asphalt road, concrete blocks, and limestone rock surfaces in a small area. Furthermore, both the pedestrian and vehicle traffic were meager in this area. The hardness of the surfaces mentioned above, was estimated by N-type Schmidt hammer test. The hammer consists of a spring-loaded piston that, when released, causes an impact on the testing surface with an energy of 2.207 N.m. The harder the impact surface is, the more the piston rebounds. According to the ASTM [43], ten Schmidt hammer tests must be done near the desired location, and the average of the tests must be determined. Then, those rebound values with more than seven units' difference from the average value must be discarded, and the average of the remaining values must be calculated. This final average value must be reported as the Schmidt hammer rebound value. The procedure outlined in ASTM [43] was followed in the present research. The obtained rebound values are shown in Table 1.

Table 1. Schmidt-hammer rebound values for impact surfaces.

Surface type	Summer	Winter
Asphalt	12.7	17.8
Concrete	35.8	36.1
Rock	49.2	33.3

The tests were conducted in two series. The first series of tests were conducted on sunny summer days with an average temperature of 36° C, while the second series were carried out on rainy winter days with an average temperature of 9° C. Table 1 shows that for the asphaltic surface, the rebound value is higher in winter than in summer. This difference can be due to the significant effect of temperature on the asphalt behavior. It is also observed that the rebound value of rock is higher in summer compared to winter. This can be attributed to the winter tests being conducted under heavy rain, which resulted in the rock surfaces being covered by a water film. This water film dissipated the impact energy, leading to a decrease in the COR. Table 1 also shows that rebound values of the concrete surface were almost constant in both summer and winter measurements. That was predictable because the strength characteristics of concrete are not affected by regular changes in temperature and water content. It should be mentioned here that the rock blocks used for tests were chosen from the insitu limestone blocks and were the same type as the rock surface.

Having selected the experiment area, some preparations were required before the tests. First, the rock blocks used in the tests were weighted and marked by blue color (Fig. 4).

Fig. 4. Marked rock blocks prior to the tests.

Next, a fixed distance was specified as the scale in the testing area. The average slope angle of impact surfaces was measured by a laser distance meter, too. The average slopes of asphalt road, concrete block, and limestone rock surface were equal to 6°, 2.5°, and 15°, respectively.

The tests were done by throwing and hitting a block of rock on the ground surface by hand while recorded by a camera with a recording rate of 60 frames per second. The camera was positioned so that both the throwing trajectory and the scale were within the frame. Additionally, the trajectory plane was aligned to be as perpendicular to the camera axis as possible. This method of conducting the tests was previously experienced and explained by other researchers [20,21].

In the next step, the recorded videos were analyzed using the motion analysis software Tracker 6.0 (developed by Jun Da High-tech Information Technology Co., Ltd. in Hefei, China). The required characteristics of the rock block motion, such as incident velocity, post-impact velocity, and pre-impact angular velocity, were determined using this software. At last, the R_v, R_t, and R_n values were calculated using Eqs. (1-3), respectively.

It is worth mentioning that the experimental program had certain limitations: some rock trajectories appeared to have out-of-plane components; rolling and sliding were the main components in some experiments, making it difficult to determine the coefficient of restitution (COR); the camera's recording rate was not high enough to accurately capture the trajectory of high-velocity impacts; and the rock blocks fragmented during some impacts.

5. Experiment results and uncertainties

A total of 931 field tests were conducted, comprising 496 tests on summer days and 435 tests on winter days. Of these tests, 571 (approximately 61%) were deemed suitable for COR calculations. Consequently, 360 tests were excluded from the analysis as their primary motion involved rolling and sliding rather than bouncing. The shape of the rock blocks significantly influenced the type of post-impact motion. For

example, if the rock blocks contacted the ground with a flat planar surface, the sliding mode was predominant. Conversely, if the rock blocks had rounded edges, rolling was the primary motion. Moreover, in some tests, the blocks' trajectories apparently deviated from the desired 2-D plane. The histograms of α_i and v_i are shown in Figs. 5 and 6, respectively.

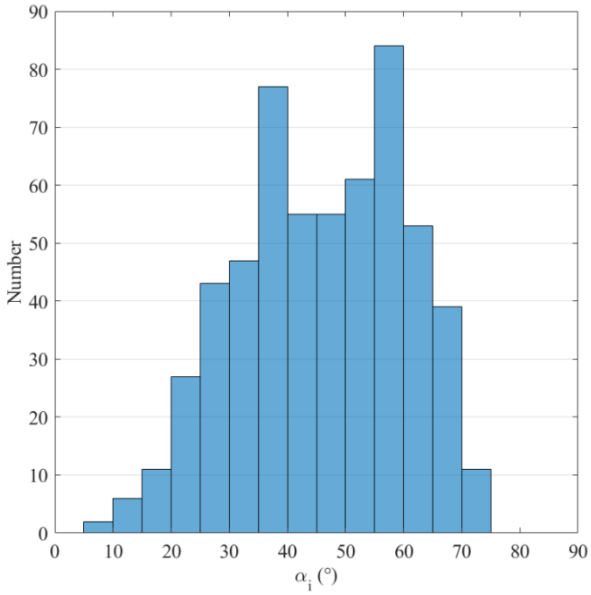

Fig. 5. Histogram of α_i.

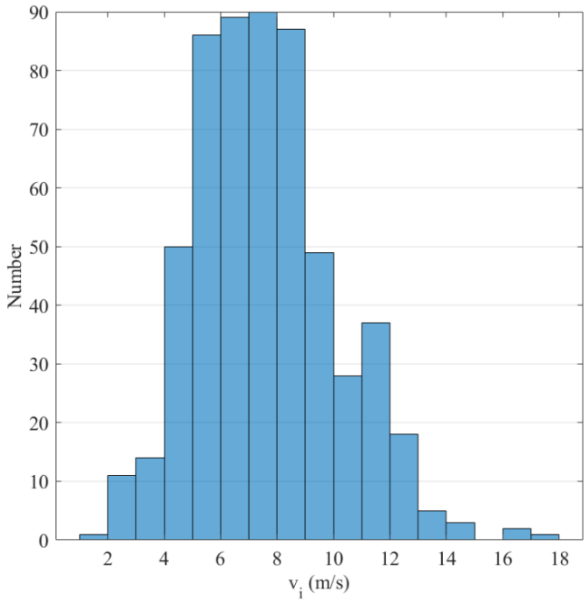

Fig. 6. Histogram of v_i.

The tests were done in such a way as to cover a wide range of input values. The α_i values were between the minimum value of 8.6° and maximum value of 74.4°, and the v_i values had a minimum of 1.9 m/s and a maximum of 17.1 m/s.

The scatterplot, accompanied by a histogram of measured R_t and R_n values, is presented in Fig. 7. Notably, two instances, both associated with concrete surfaces during summer, exhibited negative R_t values. Negative R_t values indicate that the block rebounded after impact. This could be attributed to factors such as the irregular surface of the block and a high impact angle.

Furthermore, Fig. 7 reveals instances where R_n exceeded unity. This phenomenon, also observed in previous research [12,21,22], could be attributed to irregularities in the block's shape, significant rotational energy, and low incident velocities. However, the R_v value did not exceed unity even for the highest values of R_n.

The statistical analysis of the experimental data (n = 571) provided valuable insights into the central tendency, variability, and distribution characteristics of each variable. Table 2 summarizes the key descriptive statistics for the eight variables. The interpretation of this Table is as follows:

- Impact Angle (α_i):

With a mean of 45.88° and a median of 46.60°, the distribution of impact angles is nearly symmetric, as indicated by the slight negative skewness (-0.24). The moderate standard deviation (14.20°) suggests a reasonable spread around the mean, and the kurtosis value (2.22) is close to that of a normal distribution, implying relatively light tails.

- Incident Velocity (v_i):

The mean (7.60 m/s) and median (7.42 m/s) are very similar, but a positive skew (0.51) points to a modest right tail, indicating that a

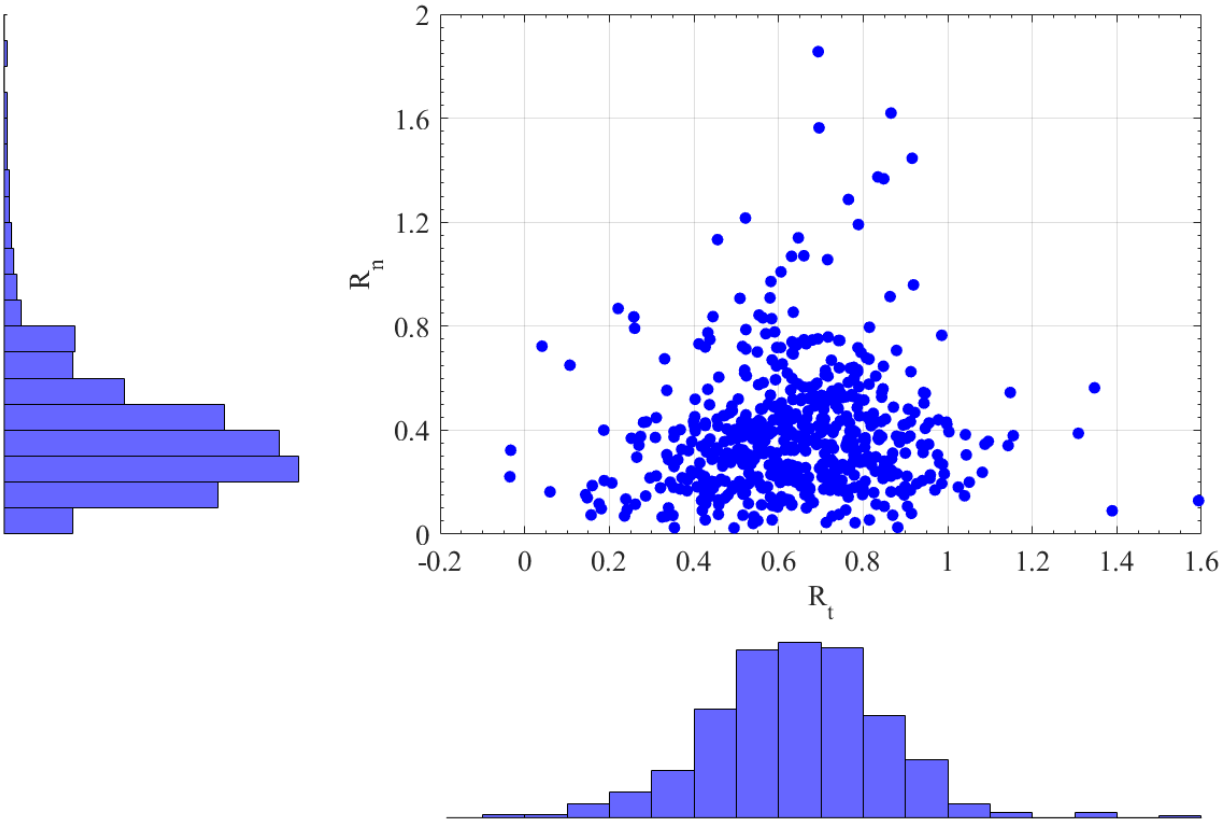

Fig. 7. The scatterplot and histogram of measured R_t and R_n values.

Table 2. Descriptive statistics for the dataset.

Parameter	Mean	Median	Standard Deviation	Skewness	Kurtosis
α_i °	45.88	46.60	14.20	-0.24	2.22
v_i (m/s)	7.60	7.42	2.47	0.51	3.43
M (kg)	1.99	1.79	0.91	0.60	3.74
ω (°/s)	772.20	627.70	627.97	1.37	5.00
R_t	0.64	0.64	0.21	0.09	4.18
R_n	0.39	0.35	0.25	2.15	11.35

R_v	0.51	0.51	0.16	0.14	3.02

few tests recorded higher velocities. The standard deviation (2.47 m/s) shows moderate variability.

- Block Mass (M):

A mean of 1.99 kg with a median of 1.79 kg and a positive skewness (0.60) suggests that while most blocks are near the central value, some are heavier. The dispersion is moderate (standard deviation = 0.91 kg).

- Angular Velocity (ω):

With a high mean of 772.20 °/s and a lower median (627.70 °/s), the positive skewness (1.37) indicates a pronounced right tail; the large standard deviation (627.97 °/s) points to high variability in the angular speeds recorded.

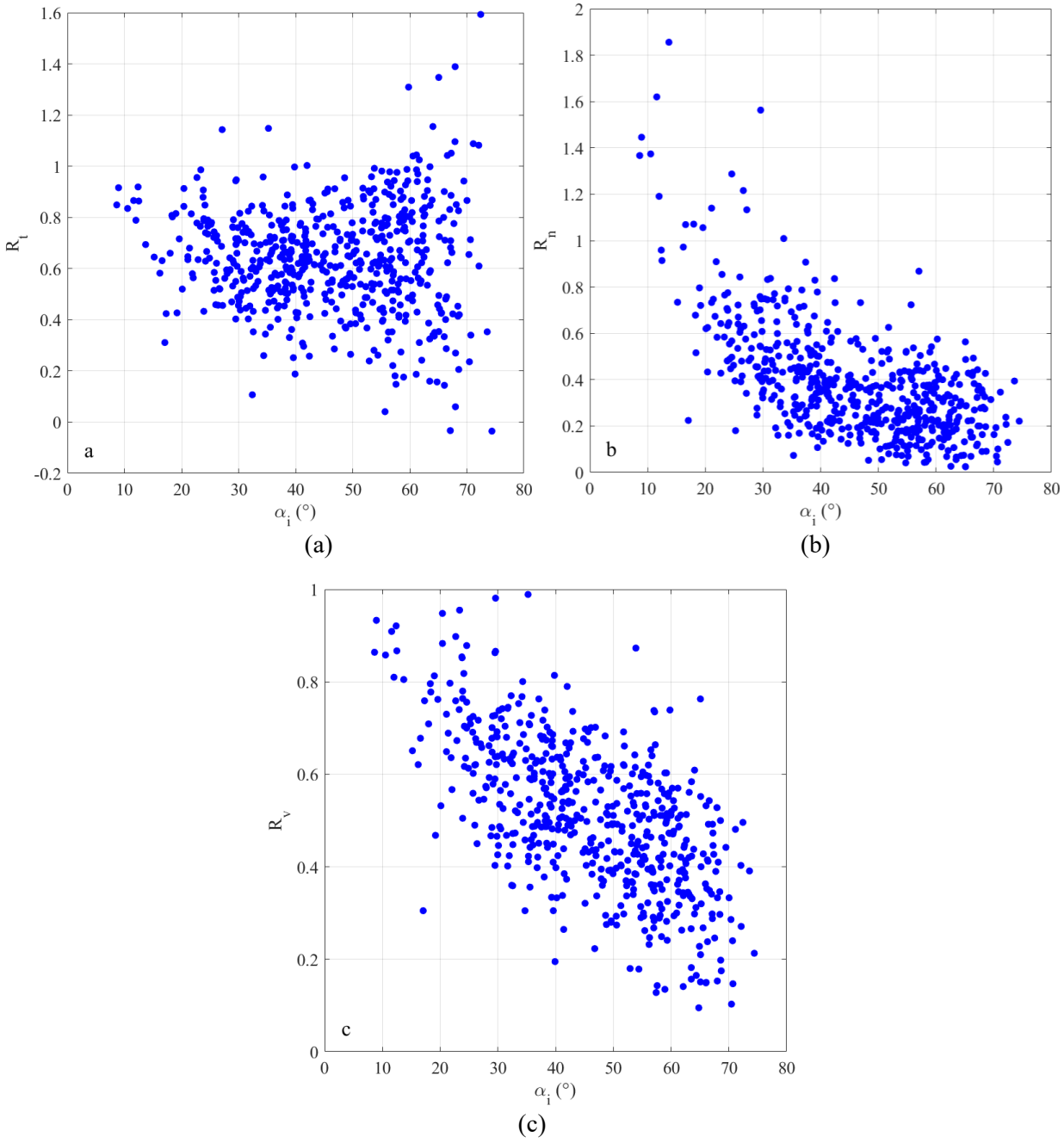

Fig. 8. Effect of α_i on (a) R_t, (b) R_n, and (c) R_v

- Coefficients of Restitution:

The tangential COR (R_t) has nearly identical mean and median (0.64) with slight skewness (0.09), suggesting a symmetric distribution with moderate variability (standard deviation = 0.21). The normal COR (R_n) exhibits high positive skewness (2.15) and a very high kurtosis (11.35), suggesting a heavy-tailed and asymmetric distribution. This may be due to physical phenomena like irregular rock shapes or measurement uncertainties.

The kinematic COR (R_v) shows a symmetric distribution (mean and median both 0.51, skewness 0.14) with low variability (standard deviation = 0.16). Variation of R_t, R_n, and R_v with α_i is shown in Fig. 8. It is seen that α_i has a decreasing effect on R_n and R_v, whereas the variation of R_t with α_i does not follow any distinct trend.

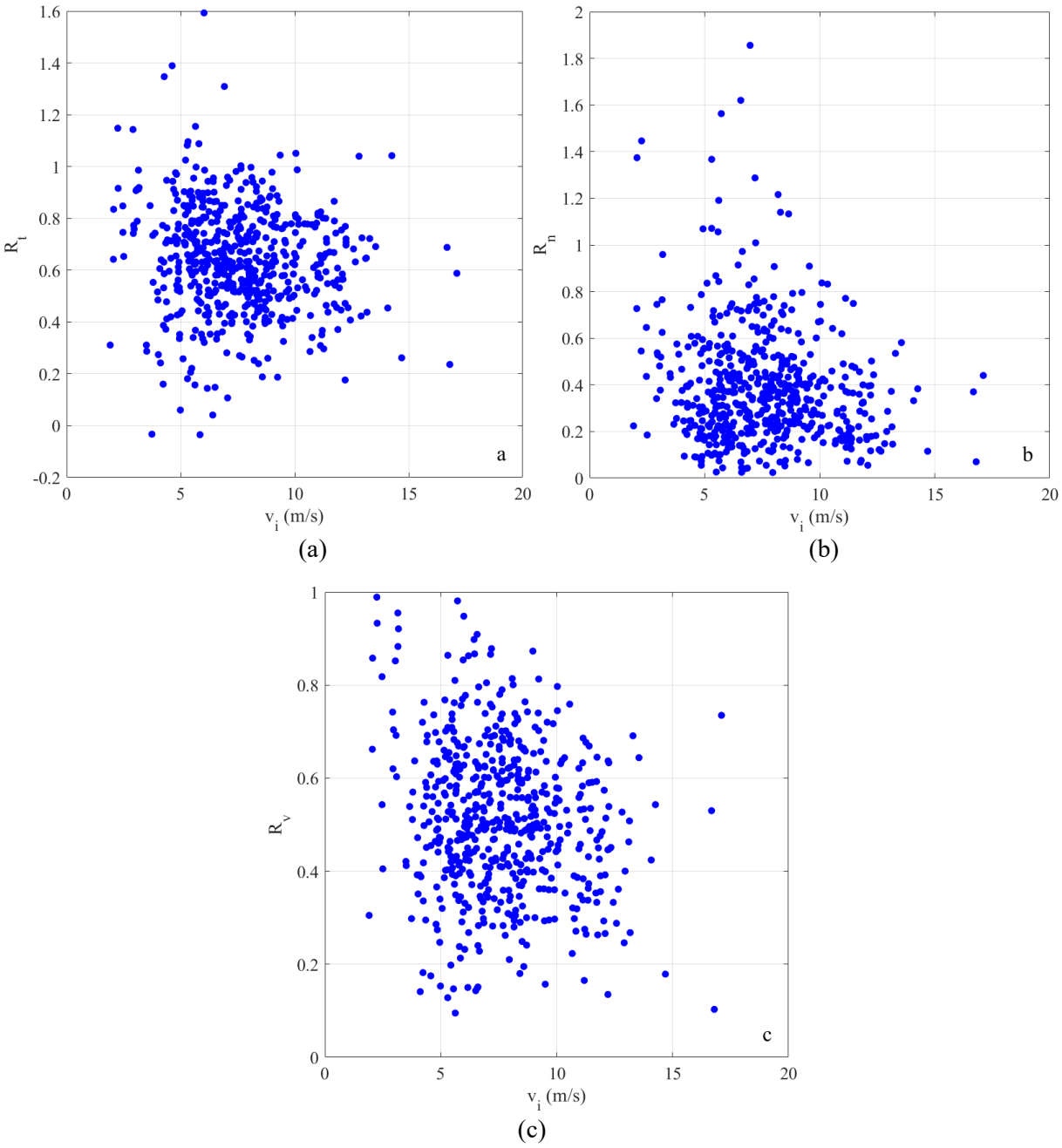

Fig. 9. Effect of v_i on (a) R_t, (b) R_n, and (c) R_v

Fig. 9 shows the variation of R_t, R_n, and R_v with v_i. It is seen that v_i has a relatively weak decreasing effect on COR values. This effect is more pronounced for R_v**.** The influence of block's mass (M) on the average value of COR, represented by $R_{t,\,avg}$, $R_{n,\,avg}$, and $R_{v,\,avg}$, is shown in Fig. 10. It is seen that the resulting plots are very scattered, and no distinct trend between the variation of mass and COR values can be recognized. It must be mentioned here that the initial mass of the blocks prior to testing was used for this purpose. Angular velocity is another parameter that may affect the COR. Variation of R_t, R_n, and R_v values with ω is shown in scatterplots of Fig. 11. It is seen that the data points do not follow any strong recognizable trend.

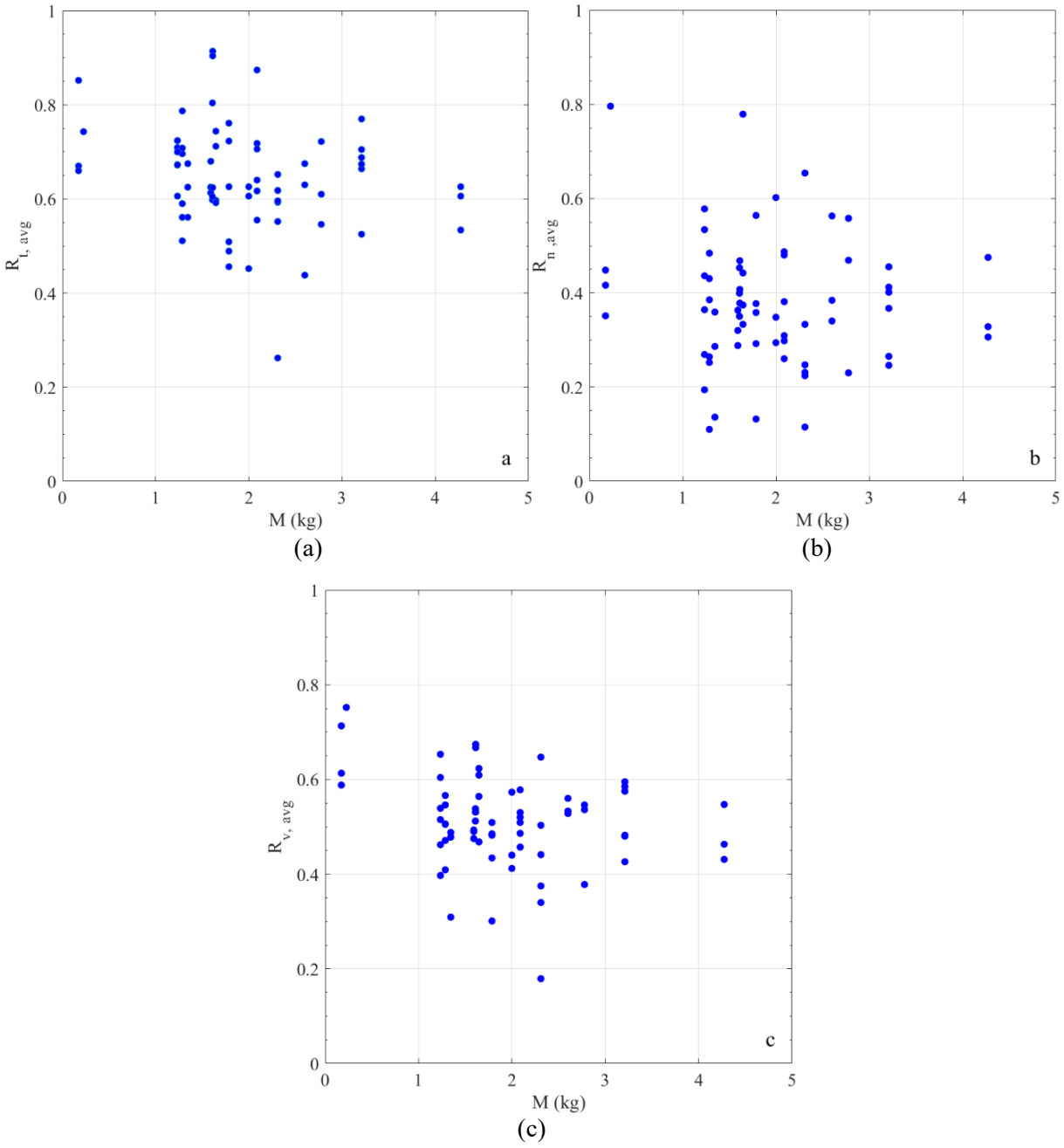

Fig. 10. Effect of M on (a) $R_{t,\,avg}$, (b) $R_{n,\,avg}$, and (c) $R_{v,\,avg}$.

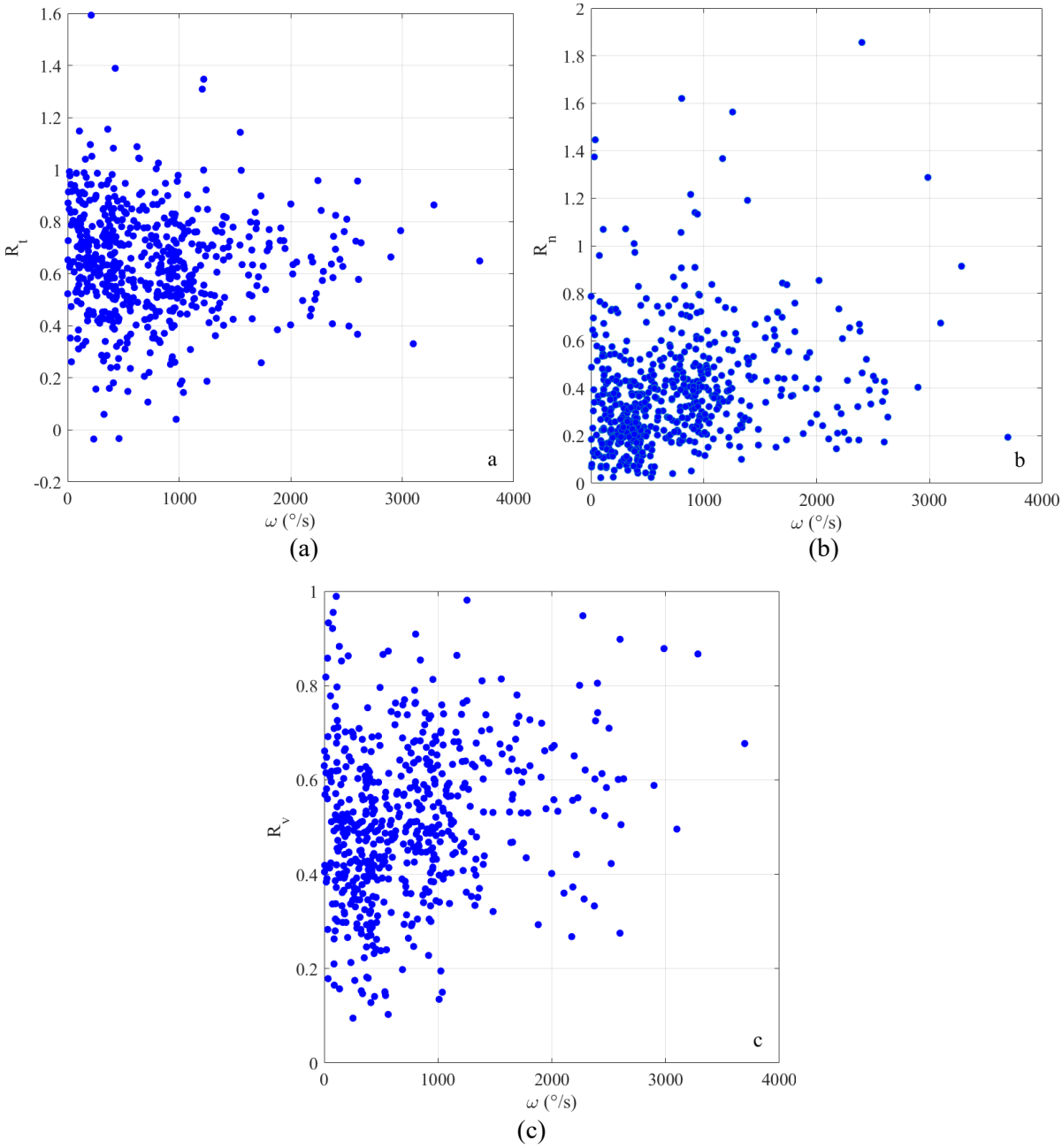

Fig. 11. Effect of ω on (a) R_t, (b) R_n, and (c) R_v.

The correlation coefficient quantifies the strength and direction of the linear relationship between two continuous variables. Its value ranges from –1 to +1. A value of +1 indicates a perfect positive correlation, meaning that as one variable increases, the other increases proportionally. A value of –1 indicates a perfect negative correlation, meaning that as one variable increases, the other decreases proportionally. A value of 0 indicates no linear correlation between the variables. The Pearson correlation coefficient between input and output variables were computed by normalizing the covariance of the variables by the product of their standard deviations, as shown in Fig. 12. It is observed that in summary, among the inputs, the impact angle has the most significant effect on the normal and kinematic CORs with its strong negative correlations. The other parameters exhibit weak relationships with the outputs, although angular velocity shows moderate positive correlations with the normal and kinematic CORs. This information is useful for guiding feature selection and understanding the model behavior in predicting rockfall dynamics.

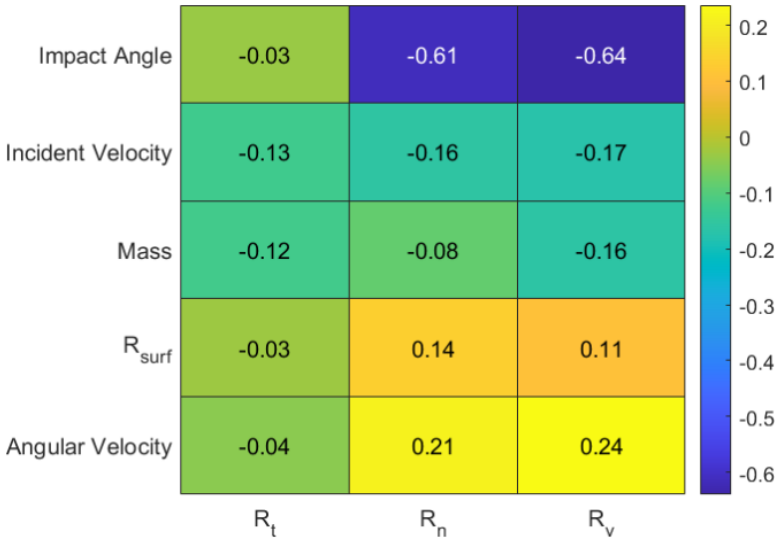

Fig. 12. The heatmap of the Pearson correlation matrix (inputs vs. outputs).

While we acknowledge that correlation analysis only captures linear dependencies and does not account for all potential interactions, the combination of scatterplots and the correlation matrix serves as an indirect but effective sensitivity analysis under the constraints of our field dataset.

To verify the reliability of our field test results, we compared the COR obtained from the subset of 129 tests on dry limestone surfaces with those reported by Robotham et al. [44] (reflected in Rocfall [9]), who performed tests under controlled conditions on dry surfaces. Robotham et al. [44] reported a R_n value of 0.315 (±0.064) and a R_t value of 0.712 (±0.116). Our tests yielded a R_n value of 0.4639 (±0.2914) and a R_t value of 0.6449 (±0.1616). Although some differences in the absolute values and variability exist, our results are within a comparable range to those of Robotham et al. [44]. The slight variations can be attributed to the inherent uncertainties in field testing, such as variations in rock shape and measurement precision. Overall, this comparison confirms that our experimental data are consistent with established values in the literature, thereby supporting the validity of our test methods and subsequent model development.

Our experience of the procedure used in this experimental study revealed that the customary method of measurement of COR values includes so many uncertainties and imprecisions, which is more apparent in the field than in the laboratory. These uncertainties would be the leading cause of several controversial results in the previous studies available in the literature. From our point of view, these uncertainties can be due to the following:

I. In the field test, you must be fortunate that the trajectory lies precisely in a 2-D plane perpendicular to the camera axis. The irregular shape of the rock block causes it to deviate from its path after hitting the surface.

II. It is entirely probable that some pieces of the block break off after impact. Consequently, the initial mass and size of the block, as measured prior to testing, would be altered after a series of impacts. A comprehensive study of fragmentation can be found in Gili et al. [45].

III. The recording rate of the camera is another influential factor. In the previous studies, a wide variety of rates, from as low as 30 frames per second [22] to as high as 1000 frames per second [17] were utilized. Nevertheless, it is not evident that what recording rate can be considered to be enough.

IV. Tracking a specified point in the motion analysis software is another thorny subject. Although the blocks were labeled with colorful points and lines, sometimes, the rotation of the blocks made the specified points hidden. This issue could be significantly more pronounced in field tests due to the

generally higher angular velocities and longer trajectories encountered compared to laboratory settings.

In this study, the authors used the capability of ANFIS to build a system for predicting the COR using the potential input variables. The properties of this inference system and the associated results are explained in the next section.

6. Resulting models

6.1. Application of ANFIS and the obtained results

In the ANFIS built for the present study, five input variables included α_i, v_i, M, R_{surf}, and ω were chosen, according to the findings of previous researchers, especially Ji et al. [17]. The Schmidt hammer rebound value has also frequently been used as an important controlling parameter in determining COR [13–20,23,45]. The subtractive clustering method [46] was utilized for generating the initial fuzzy inference system. An effective parameter in the subtractive clustering method is the range of influence (ROI). The ROI, which is a positive number less than or equal to one, represents the radius of clusters.

In the training process, a hybrid approach based on the combination of least-squares and backpropagation gradient descent methods was implemented for the optimization. In the backpropagation process, the error between the predicted output and the actual target is backpropagated (from the output end toward the input end) through the network. The parameters of the membership functions are updated using the gradient descent method, while the parameters of the output functions are updated using least-squares estimation.

This hybrid approach achieves convergence significantly faster compared to relying solely on the gradient descent method (see [28] and [47] for more details). This iterative training process continues until the error converges to a minimum value, ensuring that the model is able to accurately predict the output for new, unseen data.

Table 3. Effect of ROI on the RMSE values and number of membership functions of each input parameter.

	ROI	Number of membership functions	RMSE	
			Train	Test
R_t	0.5	7	0.185	0.201
	0.6	4	0.192	0.193
	0.7	4	0.189	0.197
	0.8	2	0.198	0.194
R_n	0.5	6	0.149	0.241
	0.6	4	0.156	0.217
	0.7	3	0.159	0.216
	0.8	3	0.161	0.265
R_v	0.5	5	0.109	0.133
	0.6	4	0.111	0.134
	0.7	3	0.112	0.129
	0.8	2	0.115	0.126

Eighty percent of the data was used in the training step, and the remaining 20% was used for testing. The effect of ROI on the number of membership functions of each input parameter and corresponding root mean square error (RMSE) is well shown in Table 3.

It is seen that, in general, as the ROI increases, the number of membership functions decreases. The ROI of 0.6 was selected for this study leading to four membership functions for each input parameter. The membership functions of input parameters for the ANFIS used for R_v prediction are shown in Fig. 13. The properties of each Gaussian membership function including its standard deviation and mean are presented

in Table 4. To evaluate the goodness of fit of the proposed ANFIS model, an F-test was conducted on the R_v testing data. The F-statistic is a measure used to evaluate the overall significance of a regression model by comparing the variance explained by the model to the variance left unexplained. It assesses whether the predictors in the model collectively contribute to explaining the variability in the observed data.

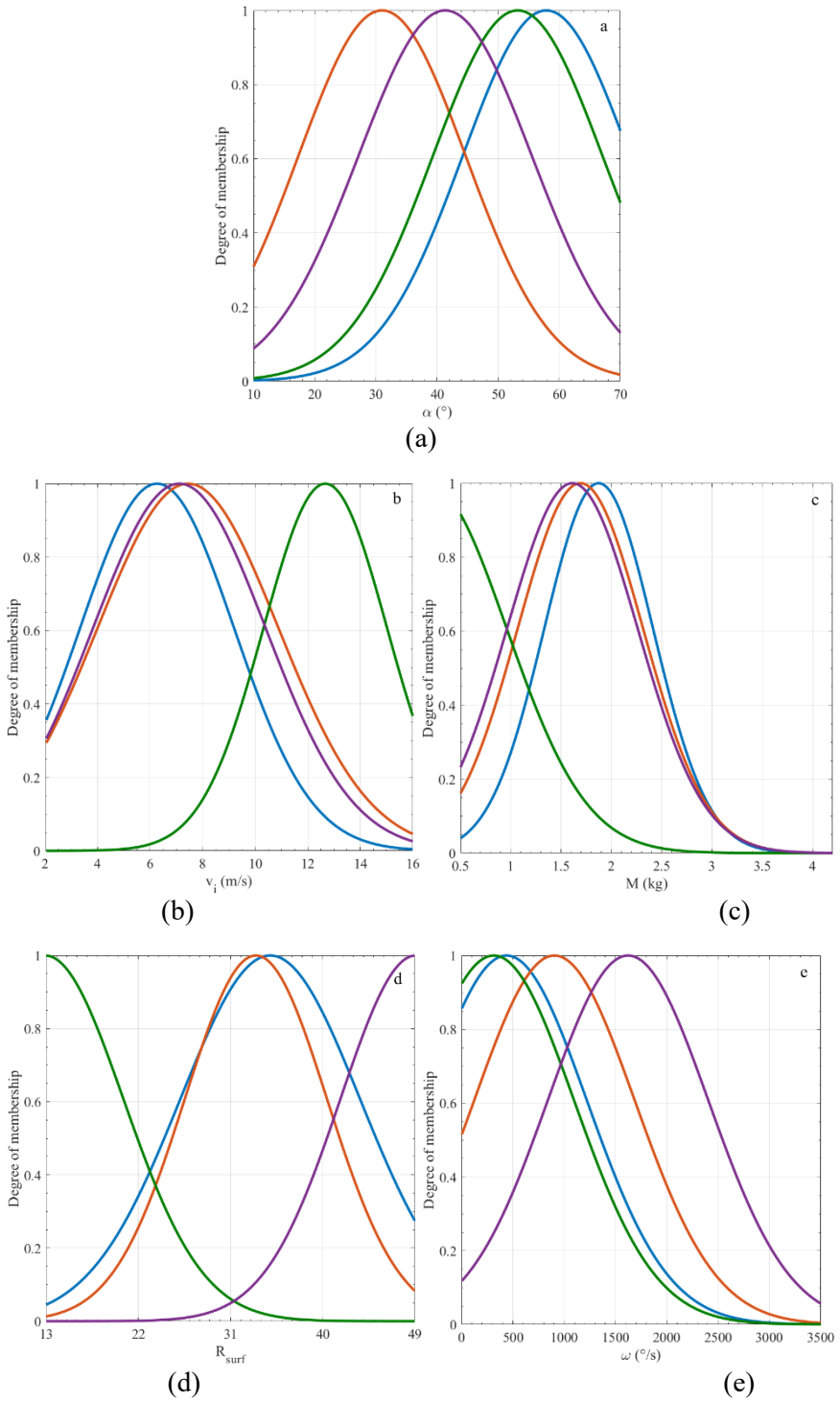

Fig. 13. Membership functions of (a) α_i, (b) v_i, (c) M, (d) R_{surf}, and (e) ω.

Table 4. Properties of membership functions.

Variable	Membership function	Standard deviation	Mean
α_i	Red	13.71	31.01
	Green	13.9	53.2

	Blue	13.69	57.87
	Purple	14.21	41.34
v_i	Red	3.45	7.45
	Green	2.354	12.67
	Blue	2.934	6.262
	Purple	3.289	7.11
M	Red	0.6242	1.691
	Green	0.7907	0.1687
	Blue	0.5413	1.873
	Purple	0.6505	1.611
R_{surf}	Red	6.956	33.49
	Green	7.653	12.91
	Blue	8.787	34.89
	Purple	7.378	49.11
ω	Red	783.3	904.7
	Green	783.3	313.8
	Blue	783.3	438.4
	Purple	783.3	1622

A larger F-statistic indicates a better fit of the model compared to a null model (with no predictors). The corresponding *p*-value indicates the likelihood of observing such an F-statistic under the null hypothesis that the model does not improve prediction. The analysis yielded an F-statistic of 82.10 ($p < 0.001$), indicating that the model explains a significant portion of the variability in the observed data compared to a null model. This result demonstrates the effectiveness of the ANFIS approach in predicting the coefficient of restitution in rockfall dynamics.

Furthermore, to provide a more comprehensive evaluation of the model's performance on R_v prediction, additional error metrics were computed on the testing dataset. The Mean Absolute Error (MAE), which quantifies the average magnitude of the prediction errors without considering their direction, was determined to be 0.1048. In addition, the maximum percentage error reached 204.47%, indicating that some outlier predictions exhibit a large discrepancy relative to the true values. To further assess prediction accuracy, we calculated a20%, defined as the percentage of predictions that fall within a 20% error margin of the observed values; in our case, 61.40% of the predictions met this criterion. Together, these performance metrics—along with the F-test results—demonstrate that the ANFIS model effectively captures the variability in the experimental data and is a robust tool for predicting the coefficient of restitution in rockfall dynamics.

Generally, the authors found the ANFIS to be an efficient tool for predicting the CORs because of its ability to take into account the uncertainties associated with this complex issue.

6.2. MARS resulting model

We trained MARS models with interaction degrees H = 1,2 on the same 571-sample dataset to determine R_v as a function five input variables, as used in the ANFIS model and selected the number of basis functions N at the point where the generalized cross-validation (GCV) curve reaches a clear "elbow." All models were grown to 50 candidate terms and then pruned via backward elimination using GCV as the selection criterion (see Eq. 13). Putting these observations together, the best model for degree =1, 2 and the corresponding statistical measures are summarized in Table 5.

Table 5. statistical metrics for MARS (H =1, 2) and ANFIS models.

Model	ANFIS	MARS (H=1)	MARS (H=2)
# BFs	--	6	8
GCV	--	0.0152	0.0144
R^2	0.4230	0.4581	0.4996
MAE	0.105	0.098	0.095
RMSE	0.134	0.121	0.118

The explicit form of the final selected model with H = 2 and 8 basis functions is:

$$R_v = 0.501964 - 0.00625294.\,\mathrm{BF1} + 0.00981479.\,\mathrm{BF2} + 0.0260959.\,\mathrm{BF3} + 0.000219565.\,\mathrm{BF4} - 0.00352035.\,\mathrm{BF5} - 0.0289935.\,\mathrm{BF6} - 2.18192 \times 10^{-6}.\,\mathrm{BF7} \quad (16)$$

where:

BF1=max(0, α_i−32.57); BF2=max(0, 32.57− α_i); BF3=max(0, 12.22−v_i); BF4=BF1×max(0, 33−R_{surf}); BF5=BF3×max(0, M−0.226); BF6=max(0, 25.5−R_{surf})×max(0, 18.39− α_i); BF7= BF1×max(0, 1207−ω);

Figure 14 plots the generalized cross-validation (GCV) error versus the number of basis functions for the degree-2 model. The GCV decreases steeply from one to eight basis functions, reflecting rapid gains in capturing the dominant nonlinear structure. From eight up to roughly 25 terms, the curve enters a broad plateau, indicating that adding more basis functions contributes progressively less to improving model performance. Beyond approximately 25 terms, the GCV rises again, signaling overfitting as the model begins to fit noise rather than the underlying signal. Therefore, we select the eight-term model at this "elbow," balancing predictive accuracy with model complexity.

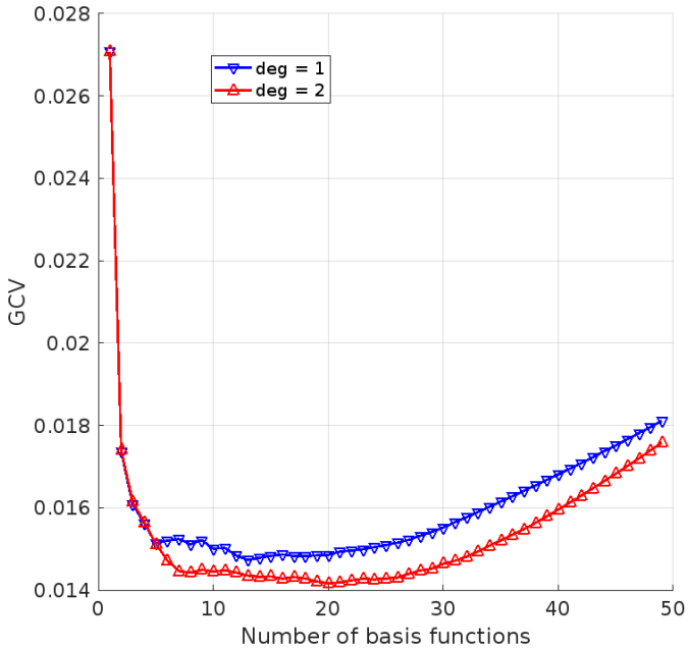

Fig. 14. Variation of GCV with number of basis functions for R_v model.

Effect of number of basis functions on R^2 and RMSE is shown in Figs. 15 and 16, respectively. It is seen that the model with H=2 has higher R^2 and lower RMSE than H=1 model, indicating its superiority.

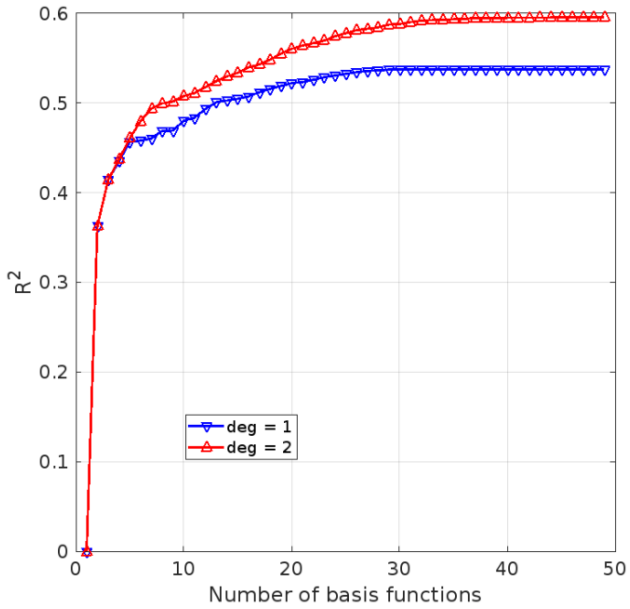

Fig. 15. Variation of R^2 with number of basis functions for R_v model.

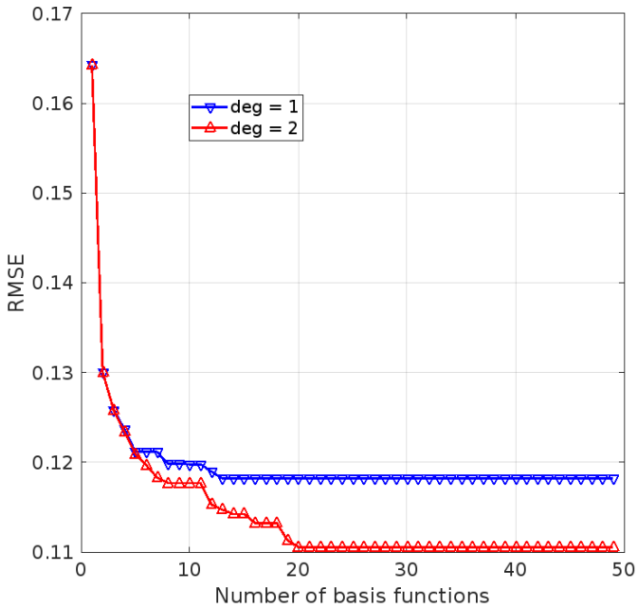

Fig. 16. Variation of RMSE with number of basis functions for R_v model.

A direct comparison on the common test set shows that MARS (degree 2, 8 basis functions) achieves MAE = 0.095 and RMSE = 0.118, while the ANFIS model yields MAE = 0.105 and RMSE = 0.134. Thus, although MARS attains marginally lower absolute errors, the improvement over ANFIS is modest. The ANFIS approach remains attractive for its rule-based learning of highly nonlinear relationships, whereas MARS offers a fully explicit formula and built-in variable importance for straightforward implementation and sensitivity analysis.

Fig. 17 overlays the test-set predictions from our ANFIS and MARS models against the measured R_v values. Both sets of points cluster tightly about the 1:1 line, reflecting that each approach captures the bulk of the variance in our field data. The root-mean-square error difference—0.134 for ANFIS vs. 0.118 for MARS—is modest, and indeed the two clouds of markers largely coincide. This close agreement underscores that both machine-learning approaches are comparably effective at predicting R_v under the substantial noise and variability of our limestone field tests. The MARS model's slight edge is more apparent in its lower overall scatter (especially at high R_v), but the performance gap would be barely distinguishable by eye on this plot.

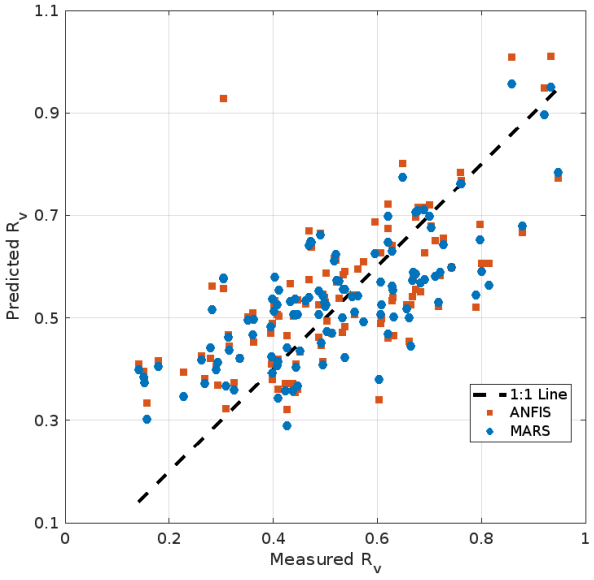

Fig. 17. Predicted vs. measured R_v values on the test set, comparing ANFIS and MARS against the 1:1 reference line (dashed).

The relative importance (RI) analysis, as shown in Fig. 18, quantifies the contribution of each predictor variable to the model's performance by measuring the increase in the generalized cross-validation error (ΔGCV) when that variable is excluded.

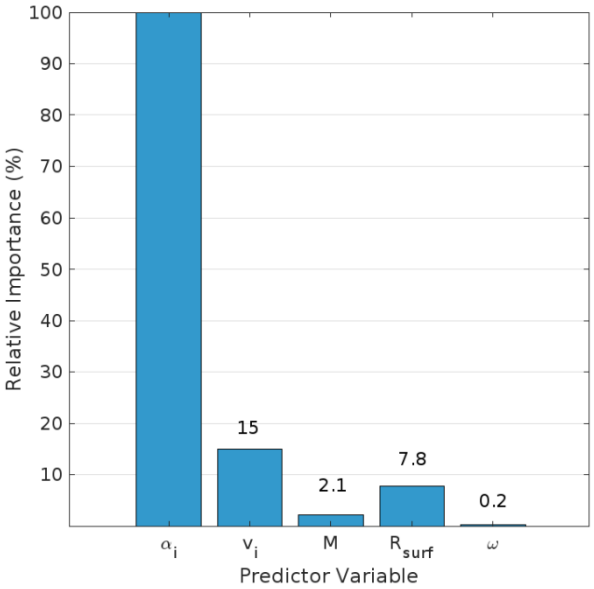

Fig. 18. Relative importance of input variables for R_v model.

In this case, α_i is the most influential variable, with a normalized RI of 100%, indicating it has the greatest impact on model accuracy. Variable v_i also contributes significantly but to a much lesser extent (about 15% relative to α_i). The predictors R_{surf} and M show moderate influence, with RI values below 8% and 3%, respectively, while ω has negligible impact on the model (near 0%). This ranking helps identify which inputs drive the model's predictions and which may be less critical.

To further analyze the internal structure of the MARS model and assess the relative contribution of each input feature, the authors performed an ANOVA-style decomposition. This technique partitions the model output into additive components, each corresponding to a specific basis function. For each BF, we report its standard deviation (STD), the associated reduction in generalized cross-validation (ΔGCV), and the input variables involved. Functions with higher standard deviation and ΔGCV values have greater impact

on the model output and its predictive performance. As shown in Table 6, the most influential basis functions are primarily associated with variable α_i, both individually and in interaction with v_i. This observation is consistent with the relative importance ranking plot, reaffirming that α_i plays the dominant role in predicting the coefficient of restitution.

Table 6. ANOVA-style decomposition of the final MARS model (degree = 2).

Function	STD	ΔGCV	Variables
1	0.0737	0.0285	α_i
1	0.0380	0.0222	α_i
3	0.0645	0.0396	α_i
4	0.0027	0.0272	α_i, v_i
5	0.0000	0.0271	α_i, v_i
6	0.1175	0.0356	α_i, v_i
7	0.0014	0.0270	α_i, v_i

To provide additional insight into the behavior of the MARS model, a parametric study was conducted. In this analysis, each input variable was varied individually across its normalized range from 0 to 1 while all other variables were held constant at their respective mean values. The resulting output predictions were plotted to visualize how each predictor influences the model's response (see Fig. 19). As shown in the figure, the predicted coefficient of restitution exhibits the most pronounced sensitivity to α_i, with a strong and nearly linear decrease in response as this variable increases — a pattern consistent with the variable's dominant relative importance score. Variable v_i also has a nonlinear but noticeable effect, reflecting secondary influence. Conversely, the curves for M, R_{surf}, and especially ω are relatively flat, indicating weak contributions to the output within the examined range. These patterns reinforce and visually validate the results of the relative importance analysis.

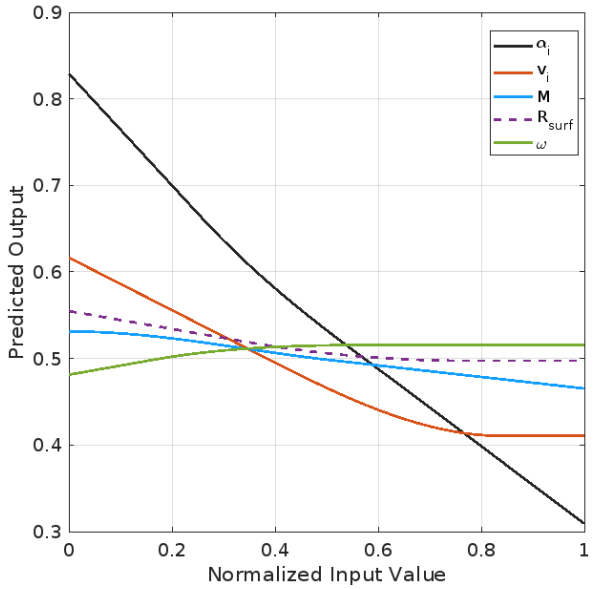

Fig. 19. Parametric study of the final MARS model (degree = 2, 8 BFs).

7. Conclusions

The primary objective of this study was to predict the coefficient of restitution (COR) for limestone in rockfall dynamics using an adaptive neuro-fuzzy inference system (ANFIS) and a Multivariate Adaptive

Regression Splines (MARS). A total of 931 field tests were conducted, and the ANFIS and MARS models were trained using five input variables: impact angle (α_i), incident velocity (v_i), block mass (M), Schmidt hammer rebound value (R_{surf}), and angular velocity (ω). Key findings from this study include:

1) The impact angle (α_i) had a decreasing effect on the normal and kinematic CORs, while no clear trend was observed for the tangential COR.

2) Incident velocity (v_i) showed a weak but consistent decreasing effect on COR values, with the effect being most pronounced for the kinematic COR (R_v).

3) A total of 571 tests were suitable for COR calculation, with the remainder discarded due to rolling, sliding, or out-of-plane motion.

4) The ANFIS model demonstrated strong predictive capability, achieving RMSE values of 0.192, 0.156, and 0.111 for the tangential, normal, and kinematic CORs, respectively, on the training dataset.

5) With degree-2 interactions and eight basis functions, MARS yields MAE ≈ 0.095 and RMSE ≈ 0.118—slightly lower absolute errors than ANFIS.

Together, ANFIS and MARS methodologies confirm that machine-learning approaches can provide accurate, field-validated COR predictions. By offering both a transparent spline-based equation and a fuzzy-rule model, this combined framework enhances both the accuracy and practical utility of COR estimates in rockfall hazard assessment.

However, the study is not without limitations. The field tests involved inherent uncertainties due to irregular rock shapes, varying surface conditions, and camera recording constraints. Future work should focus on addressing these uncertainties by incorporating advanced motion-tracking techniques and conducting further tests across a broader range of surface materials and environmental conditions.

Funding

The authors declare that no funds, grants, or other support were received during the preparation of this manuscript.

Conflicts of interest

The authors report there are no competing interests to declare.

Authors contribution statement

Amir Hossein Shafiee: Conceptualization; Investigation; Software; Writing – original draft.

Nima Aein: Investigation; Writing – review & editing.

References

[1] Matsukura Y. Rockfall at Toyohama Tunnel, Japan, in 1996: effect of notch growth on instability of a coastal cliff. Bull Eng Geol Environ 2001;60:285–9.

[2] Sarro R, Mateos RM, García-Moreno I, Herrera G, Reichenbach P, Laín L, et al. The Son Poc rockfall (Mallorca, Spain) on the 6th of March 2013: 3D simulation. Landslides 2014;11:493–503.

[3] Geniş M, Sakız U, Çolak Aydıner B. A stability assessment of the rockfall problem around the Gökgöl Tunnel (Zonguldak, Turkey). Bull Eng Geol Environ 2017;76:1237–48.

[4] Hu J, Li S, Li L, Shi S, Zhou Z, Liu H, et al. Field, experimental, and numerical investigation of a rockfall above a tunnel portal in southwestern China. Bull Eng Geol Environ 2018;77:1365–82.

[5] Shafiee AH, Falamaki A, Shafiee A, Arjmand F. Probabilistic analysis of an 80,000 m2 landslide in Shiraz, Iran. Landslides 2022;19:659–71.

[6] Thakur T, Singh K, Sharma A. A Review on Analysis and Mitigation Strategies for Landslide Risk Management: Case studies of Nainital, Satluj Valley, Pipalkoti, Jhakri, Panjpiri in Himalayan Region, India. J Min Environ 2024;15:1255–70.

[7] Romana M. New adjustment ratings for application of Bieniawski classification to slopes. Proc. Int. Symp. role rock Mech. Zacatecas, Mex., 1985, p. 49–53.

[8] Qazi A, Singh K. Rock Mass Classification Techniques and Parameters: a Review. J Min Environ 2023;14:155–78.

[9] Stevens WD. RocFall, a tool for probabilistic analysis, design of remedial measures and prediction of rockfalls. 1998.

[10] PFEIFFER TJ, BOWEN TD. Computer simulation of rockfalls. Bull Assoc Eng Geol 1989;26:135–46.

[11] Meriam JL, Kraige LG, Bolton JN. Engineering mechanics: dynamics. John Wiley & Sons; 2020.

[12] Buzzi O, Giacomini A, Spadari M. Laboratory investigation on high values of restitution coefficients. Rock Mech Rock Eng 2012;45:35–43.

[13] Ansari MK, Ahmad M, Singh R, Singh TN. Correlation between Schmidt hardness and coefficient of restitution of rocks. J African Earth Sci 2015;104:1–5.

[14] Li L, Sun S, Li S, Zhang Q, Hu C, Shi S. Coefficient of restitution and kinetic energy loss of rockfall impacts. KSCE J Civ Eng 2016;20:2297–307.

[15] Asteriou P, Tsiambaos G. Effect of impact velocity, block mass and hardness on the coefficients of restitution for rockfall analysis. Int J Rock Mech Min Sci 2018;106:41–50.

[16] Asteriou P. Effect of impact angle and rotational motion of spherical blocks on the coefficients of restitution for rockfalls. Geotech Geol Eng 2019;37:2523–33.

[17] Ji Z-M, Chen Z-J, Niu Q-H, Wang T-J, Song H, Wang T-H. Laboratory study on the influencing factors and their control for the coefficient of restitution during rockfall impacts. Landslides 2019;16:1939–63.

[18] Ji Z-M, Chen Z-J, Niu Q-H, Wang T-H, Wang T-J, Chen T-L. A calculation model of the normal coefficient of restitution based on multi-factor interaction experiments. Landslides 2021;18:1531–53.

[19] Tang J, Zhou X, Liang K, Lai Y, Zhou G, Tan J. Experimental study on the coefficient of restitution for the rotational sphere rockfall. Environ Earth Sci 2021;80:419.

[20] Asteriou P, Saroglou H, Tsiambaos G. Geotechnical and kinematic parameters affecting the coefficients of restitution for rock fall analysis. Int J Rock Mech Min Sci 2012;54:103–13.

[21] Spadari M, Giacomini A, Buzzi O, Fityus S, Giani GP. In situ rockfall testing in new south wales, australia. Int J Rock Mech Min Sci 2012;49:84–93.

[22] Ferrari F, Giani GP, Apuani T. Why can rockfall normal restitution coefficient be higher than one? Rend Online Della Soc Geol Ital 2013;24:122–4.

[23] Ji Z-M, Hu S-M, Chen Z-J, Niu Q-H, Wang T-H, Wu F-Q. Laboratory investigation of the effect of the rotational speed on the coefficient of restitution. Eng Geol 2021;292:106196.

[24] Zadeh LA. Fuzzy sets. Inf Control 1965;8:338–53.

[25] Ross TJ. Fuzzy logic with engineering applications. John Wiley & Sons; 2009.

[26] Mamdani EH. Advances in the linguistic synthesis of fuzzy controllers. Int J Man Mach Stud 1976;8:669–78.

[27] Takagi T, Sugeno M. Derivation of fuzzy control rules from human operator's control actions. IFAC Proc Vol 1983;16:55–60.

[28] Jang J-S. ANFIS: adaptive-network-based fuzzy inference system. IEEE Trans Syst Man Cybern 1993;23:665–85.

[29] Khajeh A, Mousavi SR, RAKHSHANI MM. Adaptive neural fuzzy inference system models for predicting the shear strength of reinforced concrete deep beams 2015.

[30] Ghorbani A, Ghasemi MR. Reliability and sensitivity analysis of structures using adaptive neuro-fuzzy systems. J Rehabil Civ Eng 2020;8:75–86.

[31] Polykretis C, Chalkias C, Ferentinou M. Adaptive neuro-fuzzy inference system (ANFIS) modeling for landslide susceptibility assessment in a Mediterranean hilly area. Bull Eng Geol Environ 2019;78:1173–87.

[32] Razavi-Termeh SV, Shirani K, Pasandi M. Mapping of landslide susceptibility using the combination of neuro-fuzzy inference system (ANFIS), ant colony (ANFIS-ACOR), and differential evolution (ANFIS-DE) models. Bull Eng Geol Environ 2021;80:2045–67.

[33] Shafiee AH, Oulapour M, Abdlkadhim MAA. Stability of subsea circular tunnels using finite element limit analysis and adaptive neuro-fuzzy inference system. Earth Sci Informatics 2024;17:2417–27.

[34] Friedman JH. Multivariate adaptive regression splines. Ann Stat 1991;19:1–67.

[35] Gan Y, Duan Q, Gong W, Tong C, Sun Y, Chu W, et al. A comprehensive evaluation of various sensitivity analysis methods: A case study with a hydrological model. Environ Model \& Softw 2014;51:269–85.

[36] Shafiee AH, Neamani AR, Eskandarinejad A, Hosseini R, Gholami A. Undrained stability of wide rectangular subsea tunnels using finite element limit analysis and multivariate adaptive regression splines. Earth Sci Informatics 2025;18:60.

[37] Eskandarinejad A, Shiau J, Lai VQ, Keawsawasvong S. Predicting uplift capacity of group anchors in sand using 3D FELA and MARS. Mar Georesources \& Geotechnol 2025;43:607–21.

[38] Ghanizadeh AR, Safi Jahanshahi F, Ziayi A. Presenting a Model for Predicting CBR and UCS of Expensive Soil Stabilized with Hydrated Lime Activated with Rice Husk Ash Using the Hybrid MARS-EBS Method. Road 2025;33:45–66.

[39] Ghanizadeh AR, Ghanizadeh A, Asteris PG, Fakharian P, Armaghani DJ. Developing bearing capacity model for geogrid-reinforced stone columns improved soft clay utilizing MARS-EBS hybrid method. Transp Geotech 2023;38:100906.

[40] Ghanizadeh AR, Safi Jahanshahi F, Khalifeh V, Jalali F. Predicting flow number of asphalt mixtures based on the marshall mix design parameters using multivariate adaptive regression spline (MARS). Int J Transp Eng 2020;7:433–48.

[41] Ghanizadeh AR, Fakhri M. Prediction of frequency for simulation of asphalt mix fatigue tests using MARS and ANN. Sci World J 2014;2014:515467.

[42] Fakharian P, Nouri Y, Ghanizadeh AR, Jahanshahi FS, Naderpour H, Kheyroddin A. Bond strength prediction of externally bonded reinforcement on groove method (EBROG) using MARS-POA. Compos Struct 2024;349:118532.

[43] D-14 A. Standard Test Methods for Determination of Rock Hardness by Rebound Hammer Method, American Society for Testing and Materials West Conshohocken, PA, USA; 2014.

[44] Robotham ME, Wang H, Walton G. Assessment of risk from rockfall from active and abandoned quarry slopes. Trans Inst Min Metall Sect A Min Ind 1995;104.

[45] Gili JA, Ruiz-Carulla R, Matas G, Moya J, Prades A, Corominas J, et al. Rockfalls: Analysis of the block fragmentation through field experiments. Landslides 2022;19:1009–29.

[46] Chiu SL. Fuzzy model identification based on cluster estimation. J Intell Fuzzy Syst 1994;2:267–78.

[47] Jang J-SR, Sun C-T, Mizutani E. Neuro-fuzzy and soft computing-a computational approach to learning and machine intelligence [Book Review]. IEEE Trans Automat Contr 1997;42:1482–4.